Electronic Supplementary Information (ESI†)

Covalent-doping of Ni and P for 1T–enriched MoS_2 bifunctional 2D-nanostructures with active basal planes and expanded interlayers boosting electrocatalytic water splitting

Uday Narayan Pan[a], Thangjam Ibomcha Singh[a], Dasu Ram Paudel[a], Chandan Chandru Gudal[a], Nam Hoon Kim[a]*, Joong Hee Lee[a,b]*

[a]Advanced Materials Institute of BIN Convergence Technology (BK21 Plus Global) and Department of BIN Convergence Technology, Jeonbuk National University, Jeonju, Jeonbuk, 54896, Republic of Korea.

[b]Carbon Composite Research Centre, Department of Polymer-Nano Science and Technology, Jeonbuk National University, Jeonju, Jeonbuk, 54896, Republic of Korea.

Materials: sodium molybdate dihydrate [$Na_2MoO_4.2H_2O$], nickel(II) acetate tetrahydrate [$Ni(OCOCH_3)_2{\cdot}4H_2O$], L-Cysteine [$HSCH_2CH(NH_2)CO_2H$] and sodium phosphate monobasic [NaH_2PO_4] were purchased from Sigma-Aldrich, USA. KOH (potassium hydroxide) was procured from Samchun Chemical Co. Ltd, South Korea. Carbon cloth (CC) was obtained from Hesenbio Ltd. Shanghai, China. Obtained chemicals were then directly used for the synthesis of the catalysts (no further purifications were done)

Instruments: JEOL-JSM-6701F field emission scanning electron microscope was used for acquiring the FE-SEM images of all the samples. Jeol-JEM-2200 transmission electron microscope was used for acquiring TEM images, high-resolution TEM images and scanning TEM images of all the samples. X–ray photoelectron spectroscopic study of the samples was done using a Theta Probe X-ray photoelectron spectrometer (Maker: Thermo Fisher Scientific Inc., UK). Micromeritics-ASAP 2020 surface area and porosity analyzer was used for nitrogen adsorption–desorption study. Powder X-ray diffraction pattern of all the samples were obtained using Rigaku TTRX3 powder X-ray diffractometer. Electrochemical performances were measured using an electrochemical workstation CH660E (maker: CH Instruments, Inc., USA). Electrochemical impedance spectroscopic measurements were done using the same electrochemical workstation with AC voltage of amplitude 5 mV in frequency range 0.01 Hz to 100 kHz. The elemental compositions of the prepared samples were determined from inductively coupled plasma-optical emission spectrometry elemental (ICP-OES) and atomic absorption spectroscopy (AAS) measurements

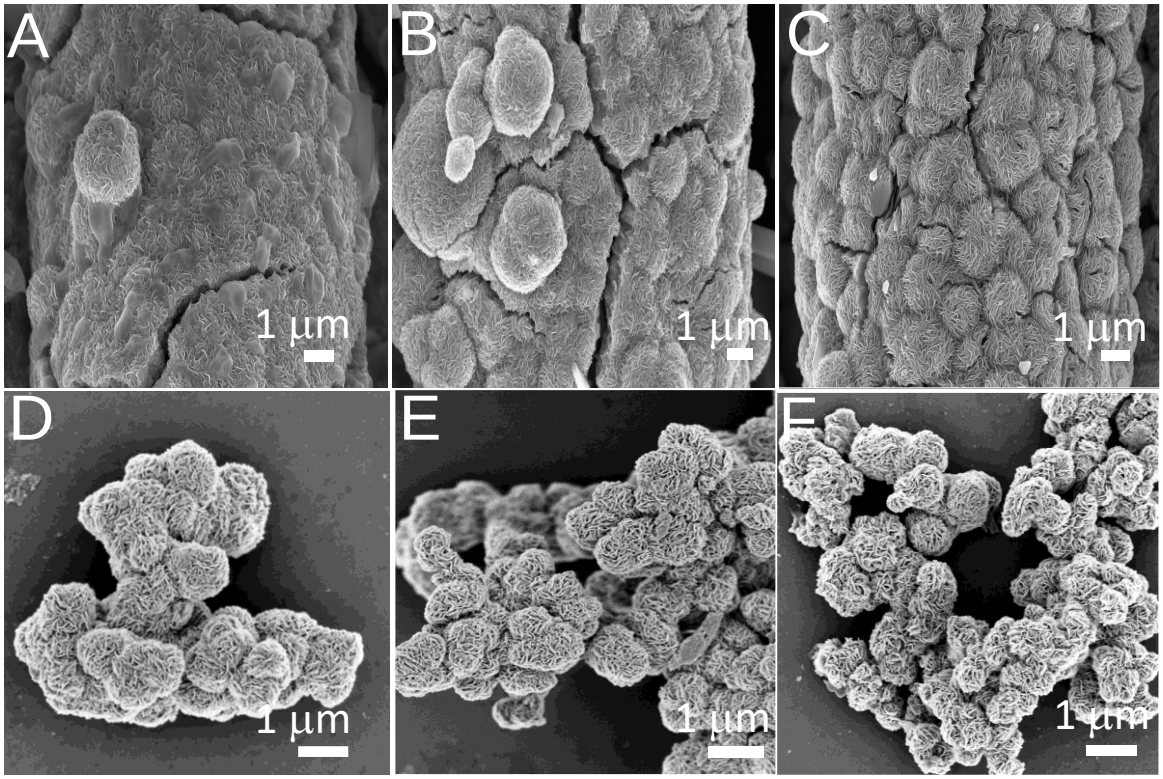

Fig. S1. FE–SEM image of **(A)** MoS_2 **(B)** Ni–doped and intercalated MoS_2 (**C**) P–doped MoS_2 nanosheets grown on carbon cloth. FE–SEM image of **(D)** MoS_2 **(E)** Ni–doped and intercalated MoS_2 (**F**) P–doped MoS_2 nanoflowers.

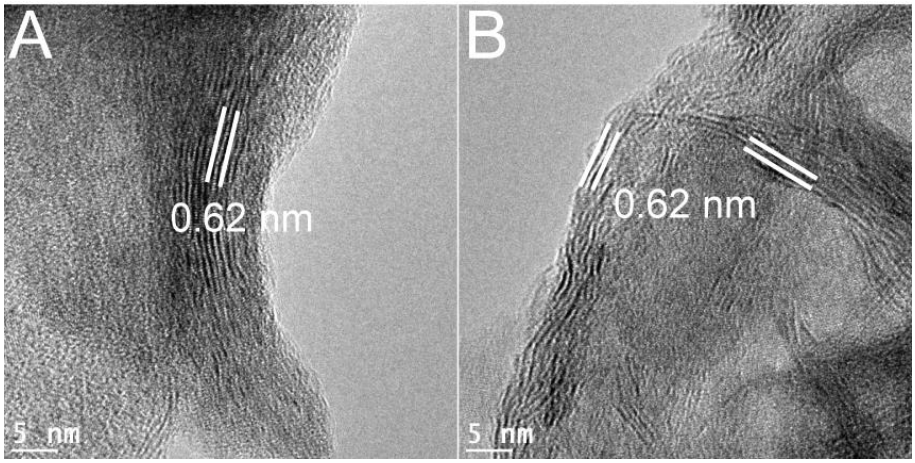

Fig. S2. TEM images of the pristine MoS_2 showing interlayer spacing.

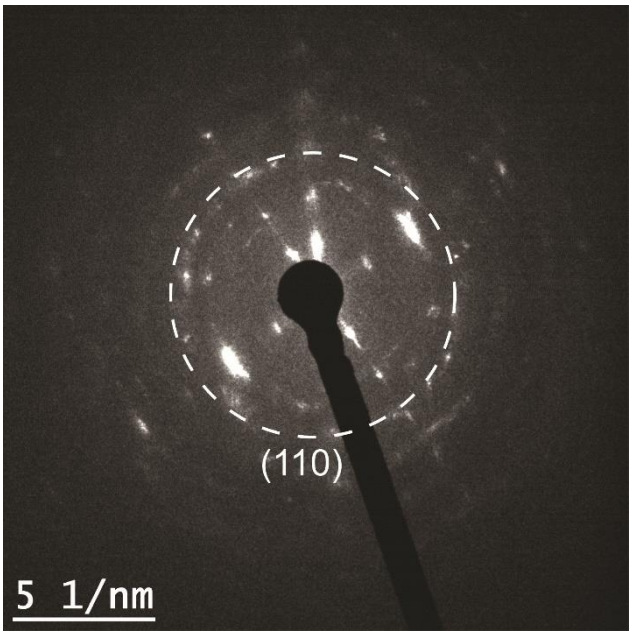

Fig. S3. Selected area electron diffraction (SAED) pattern of the 1T–$Ni_{0.2}Mo_{0.8}S_{1.8}P_{0.2}$ NFs.

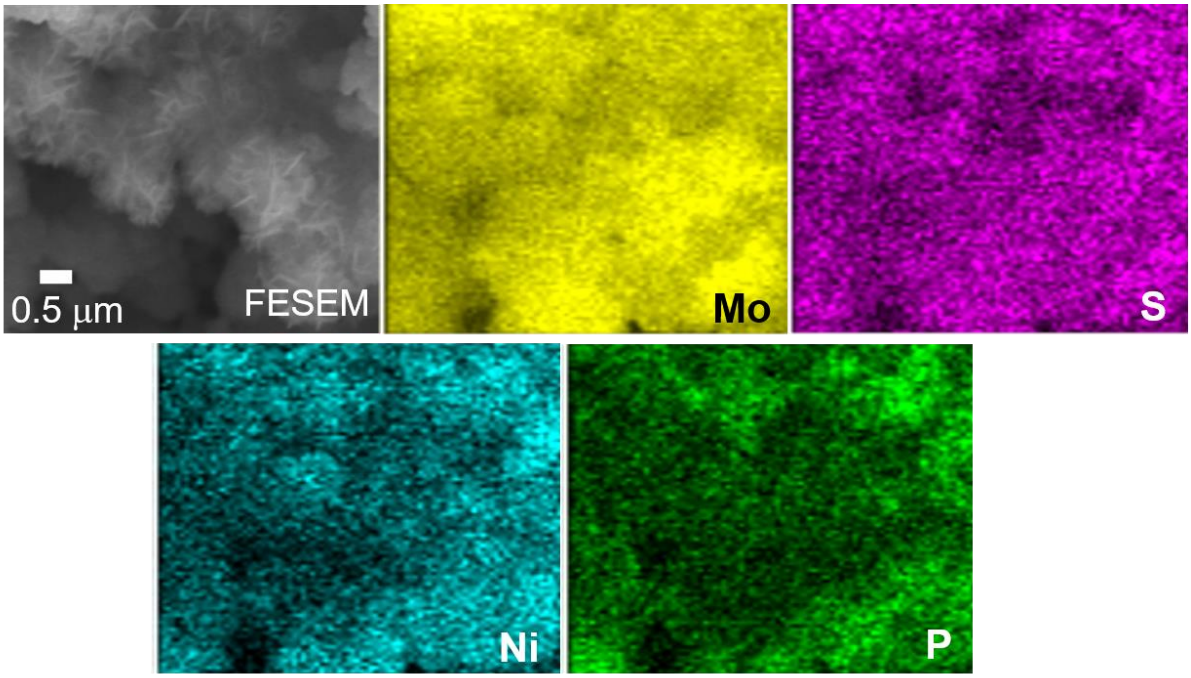

Fig. S4. FE-SEM-EDS elemental mapping of 1T–$Ni_{0.2}Mo_{0.8}S_{1.8}P_{0.2}$ NFs.

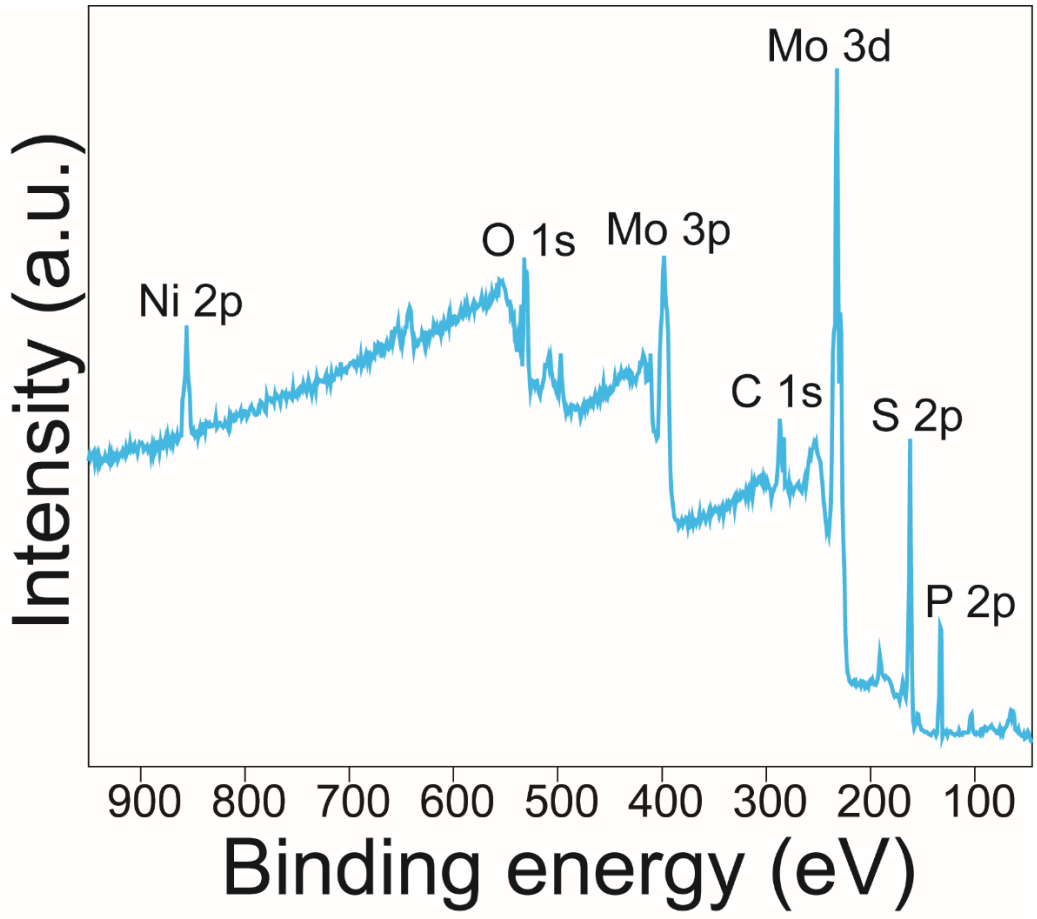

Fig. S5. XPS survey spectrum of 1T–$Ni_{0.2}Mo_{0.8}S_{1.8}P_{0.2}$ NFs.

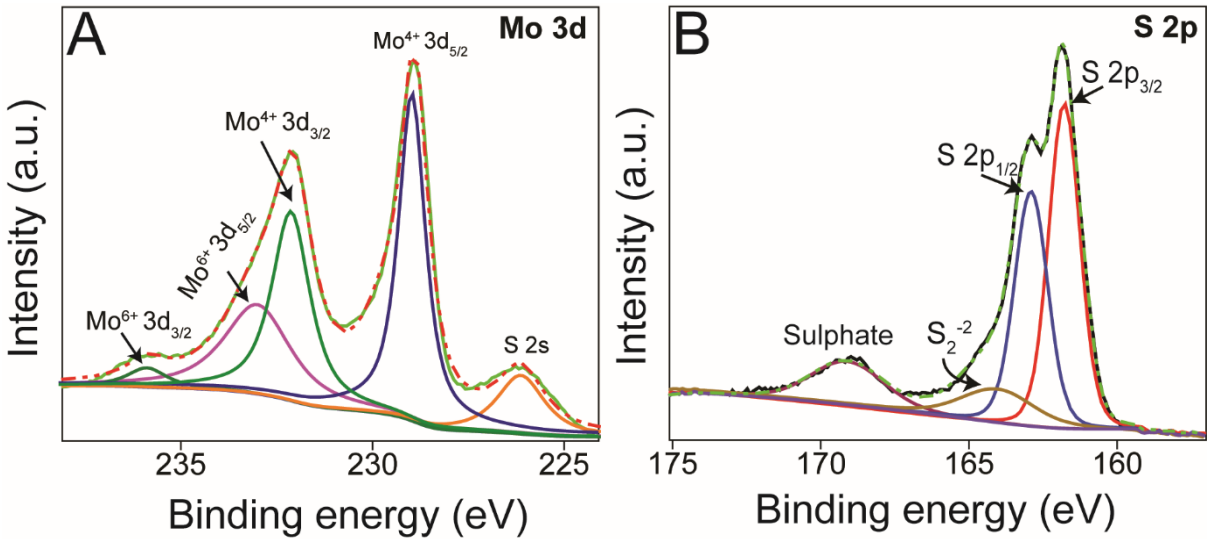

Fig. S6. High resolution X-ray photoelectron spectroscopy (XPS) plot of (**A**) Mo 3d and (**B**) S 2p for the pristine MoS_2.

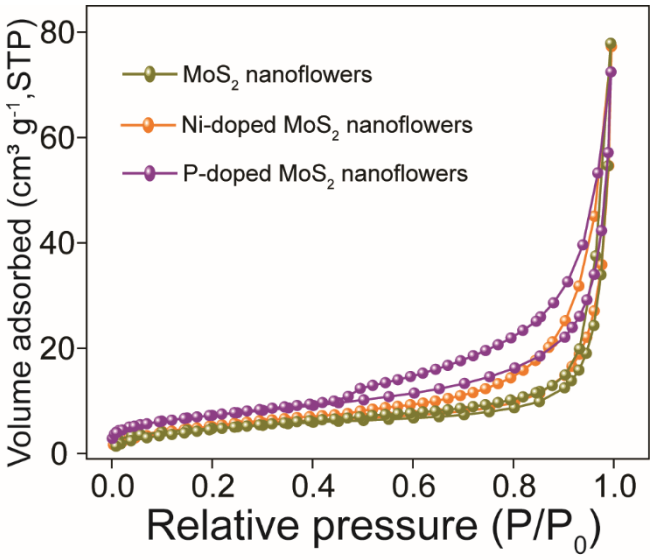

Fig. S7. N_2 adsorption-desorption isotherms of MoS_2, Ni-doped and intercalated MoS_2 and P-doped MoS_2 nanoflowers.

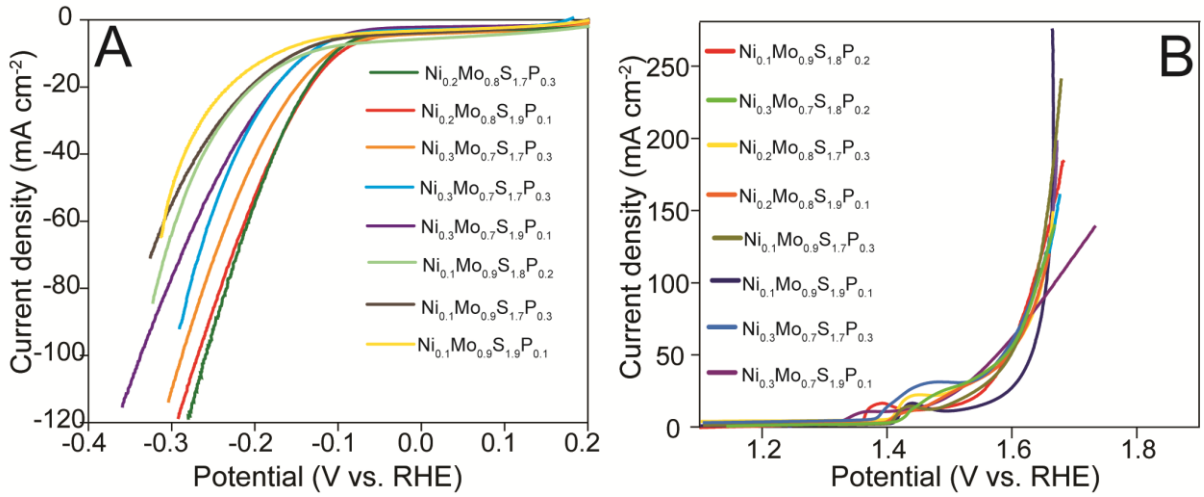

Fig. S8. (A) Linear–sweep voltammetry (LSV) measurements for hydrogen evolution reaction (HER) of $Ni_{0.1}Mo_{0.9}S_{1.8}P_{0.2}$, $Ni_{0.3}Mo_{0.7}S_{1.8}P_{0.2}$, $Ni_{0.2}Mo_{0.8}S_{1.7}P_{0.3}$, $Ni_{0.2}Mo_{0.8}S_{1.9}P_{0.1}$, $Ni_{0.1}Mo_{0.9}S_{1.7}P_{0.3}$, $Ni_{0.1}Mo_{0.9}S_{1.9}P_{0.1}$, $Ni_{0.3}Mo_{0.7}S_{1.7}P_{0.3}$, $Ni_{0.3}Mo_{0.7}S_{1.9}P_{0.1}$ and **(B)** Linear–sweep voltammetry (LSV) measurements towards oxygen evolution reaction (OER) of $Ni_{0.1}Mo_{0.9}S_{1.8}P_{0.2}$, $Ni_{0.3}Mo_{0.7}S_{1.8}P_{0.2}$, $Ni_{0.2}Mo_{0.8}S_{1.7}P_{0.3}$, $Ni_{0.2}Mo_{0.8}S_{1.9}P_{0.1}$, $Ni_{0.1}Mo_{0.9}S_{1.7}P_{0.3}$, $Ni_{0.1}Mo_{0.9}S_{1.9}P_{0.1}$, $Ni_{0.3}Mo_{0.7}S_{1.7}P_{0.3}$, $Ni_{0.3}Mo_{0.7}S_{1.9}P_{0.1}$.

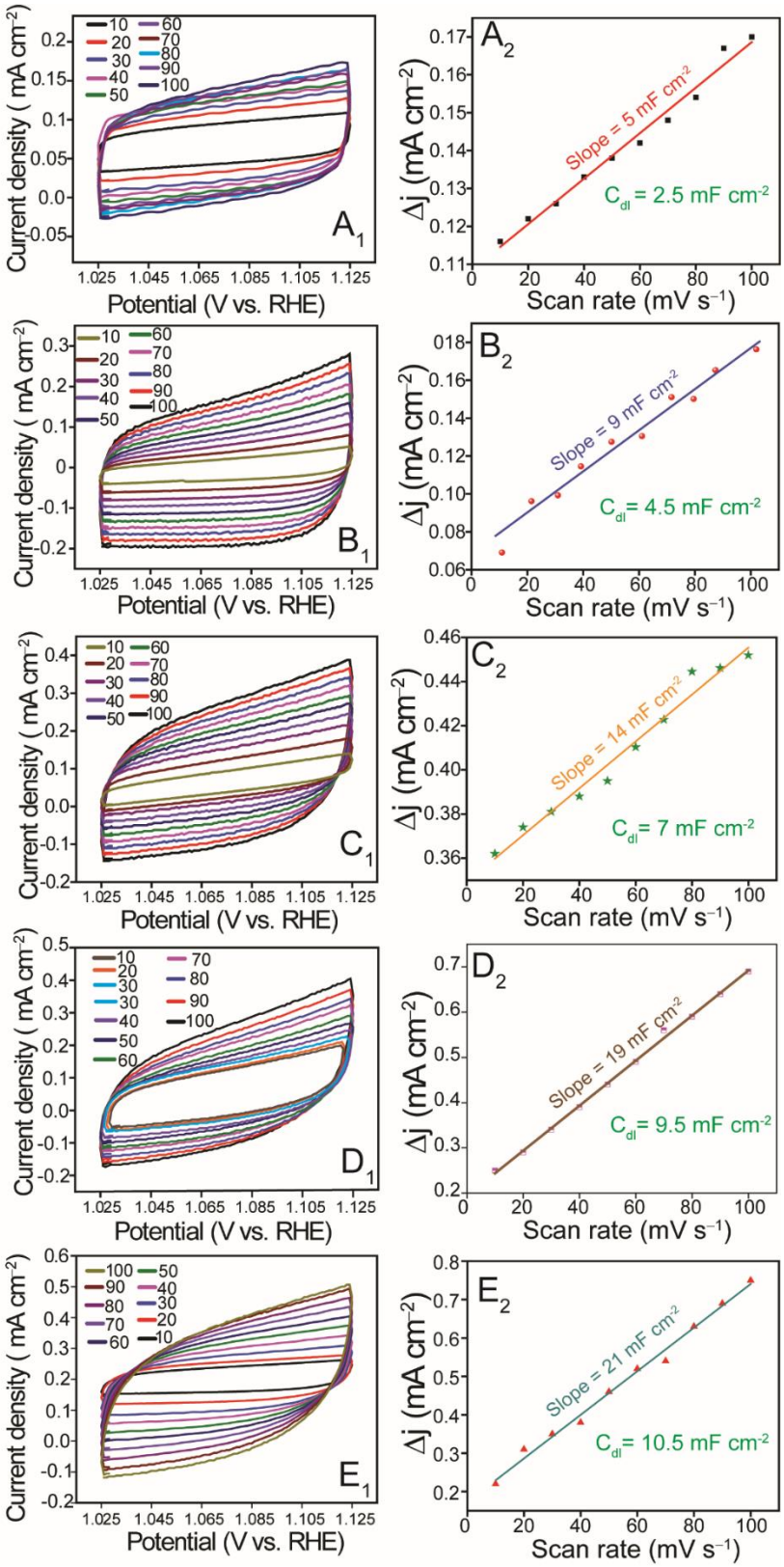

Fig. S9. Cyclic voltammograms at different scan rates of (A_1) MoS_2 (B_1) P–doped MoS_2 (C_1) Ni–doped MoS_2 (D_1) 1T–$Ni_{0.2}Mo_{0.8}S_{1.8}P_{0.2}$ NFs (E_1) 1T–$Ni_{0.2}Mo_{0.8}S_{1.8}P_{0.2}$ NS/CC. Corresponding scan rate dependent current densities of (A_2) MoS_2 (B_2) P–doped MoS_2 (C_2) Ni–doped MoS_2 (D_2) 1T–$Ni_{0.2}Mo_{0.8}S_{1.8}P_{0.2}$ NFs (E_2) 1T–$Ni_{0.2}Mo_{0.8}S_{1.8}P_{0.2}$ NS/CC.

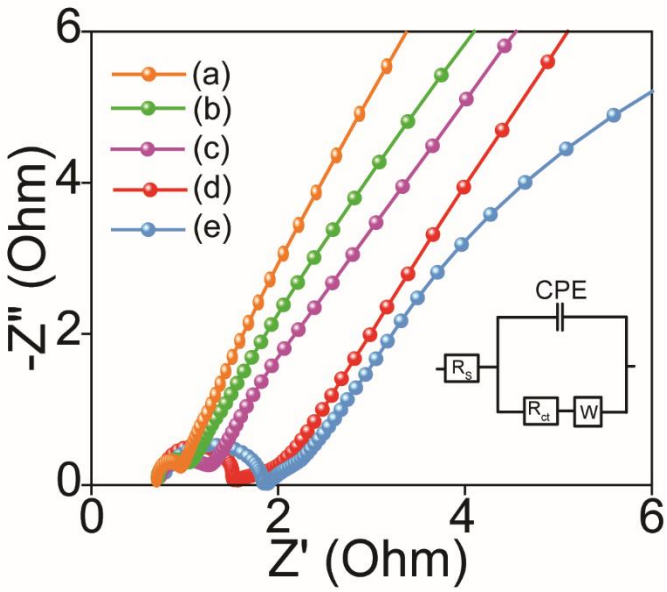

Fig. S10. Spectra of (a)1T–$Ni_{0.2}Mo_{0.8}S_{1.8}P_{0.2}$ NS/CC (b)1T–$Ni_{0.2}Mo_{0.8}S_{1.8}P_{0.2}$ NFs (c) Ni–doped MoS_2 (d) P–doped MoS_2 (e) MoS_2.

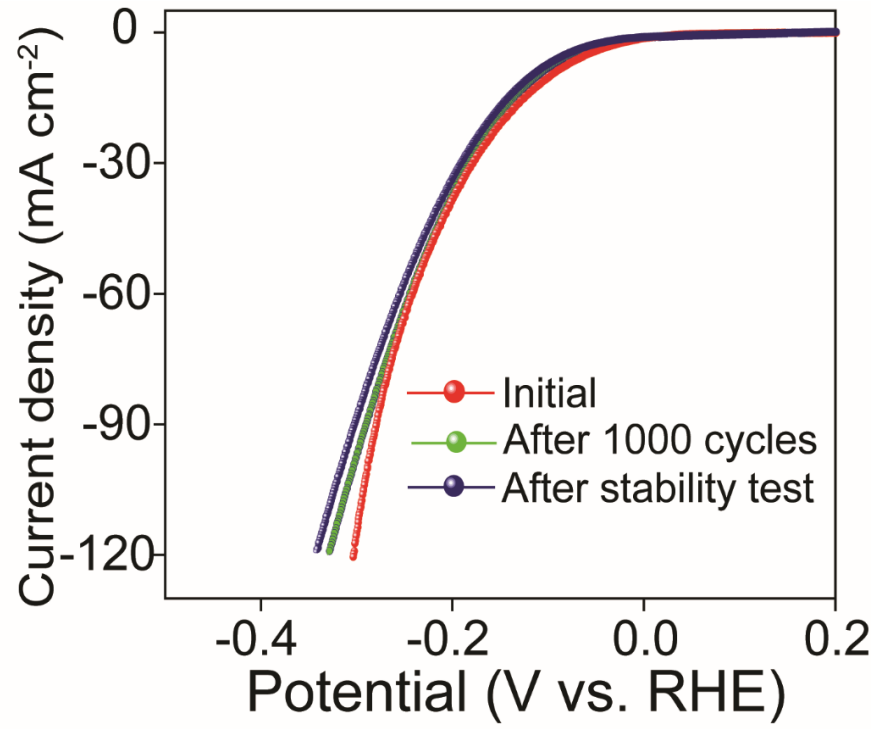

Fig. S11. Linear–sweep voltammetry (LSV) measurements towards hydrogen evolution reaction of 1T–$Ni_{0.2}Mo_{0.8}S_{1.8}P_{0.2}$ NFs before and after chronopotentiometric stability test and 1,000 consecutive CV cycles.

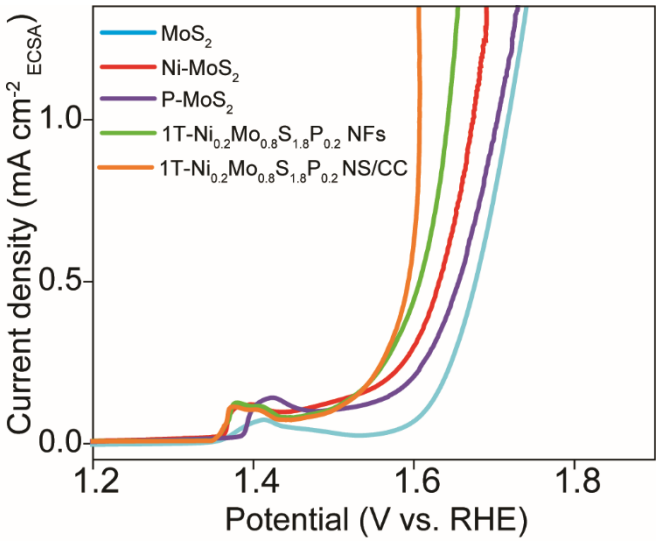

Fig. S12. ECSA normalized Linear–sweep voltammetry (LSV) measurements towards oxygen evolution reaction (OER) of MoS_2, P-doped MoS_2, Ni-doped MoS_2, 1T-$Ni_{0.2}Mo_{0.8}S_{1.8}P_{0.2}$ NFs and 1T-$Ni_{0.2}Mo_{0.8}S_{1.8}P_{0.2}$ NS/CC.

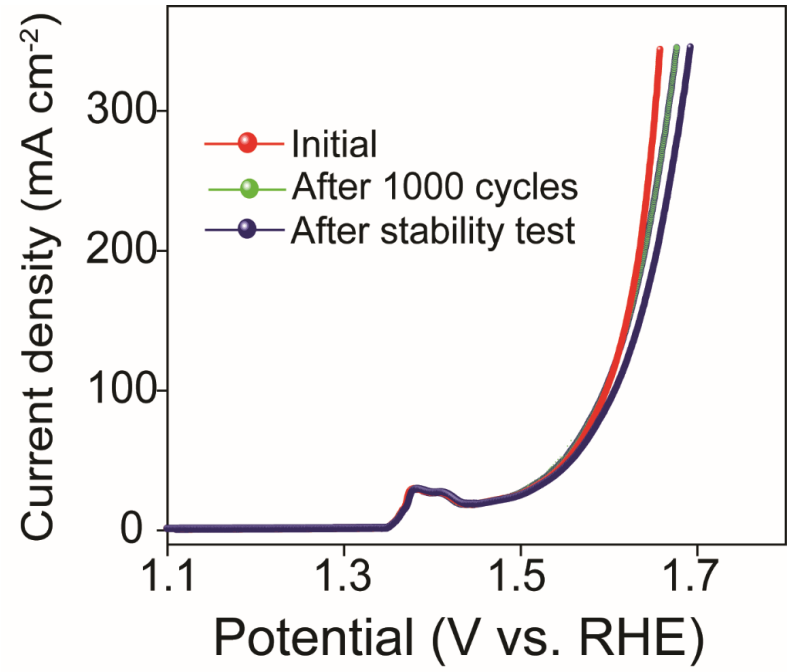

Fig. S13. Linear–sweep voltammetry (LSV) measurements towards oxygen evolution reaction of 1T–$Ni_{0.2}Mo_{0.8}S_{1.8}P_{0.2}$ NFs after chronopotentiometric stability test and 1,000 consecutive CV cycles.

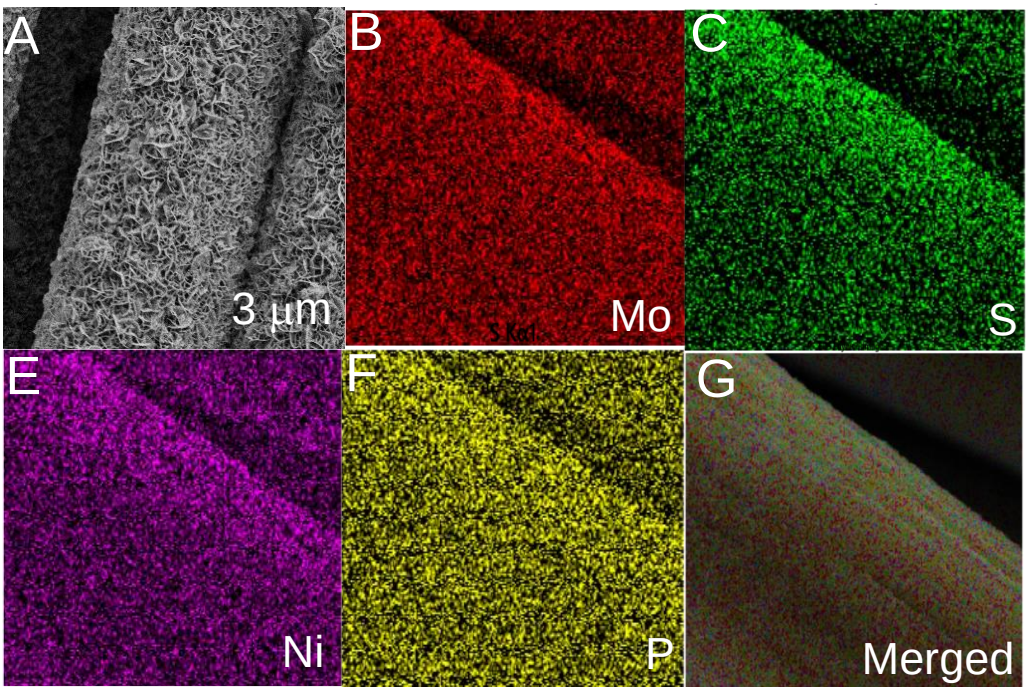

Fig. S14. (A) FESEM image. (B-G) Elemental mapping corresponding to Mo, S, Ni an d P, respectively of 1T-$Ni_{0.2}Mo_{0.8}S_{1.8}P_{0.2}$ NS/CC after long-term chronoamperometric st ability test of the device showing no significant change in the structure and elemental composition of the catalyst.

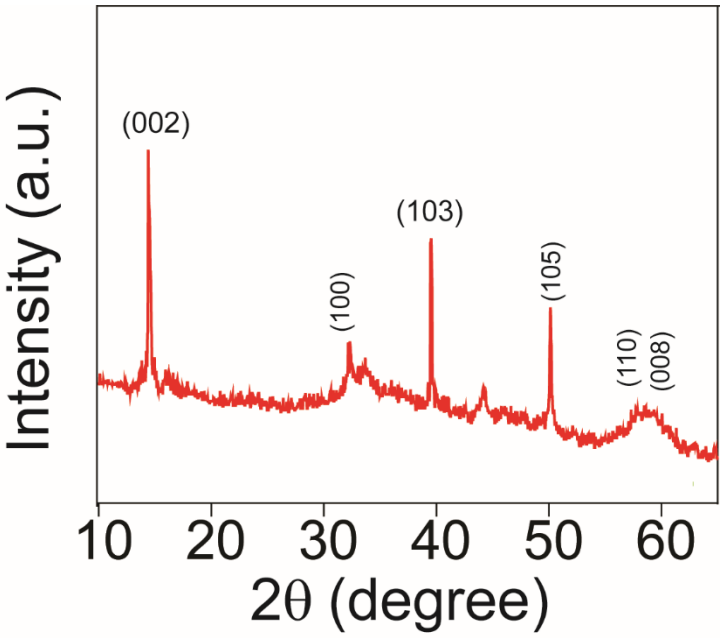

Fig. S15. X-ray powder diffraction (XRD) pattern of 1T-$Ni_{0.2}Mo_{0.8}S_{1.8}P_{0.2}$ after long-term c hronoamperometric stability test of the device showing no significant change in the cr ystallographic nature of the catalyst.

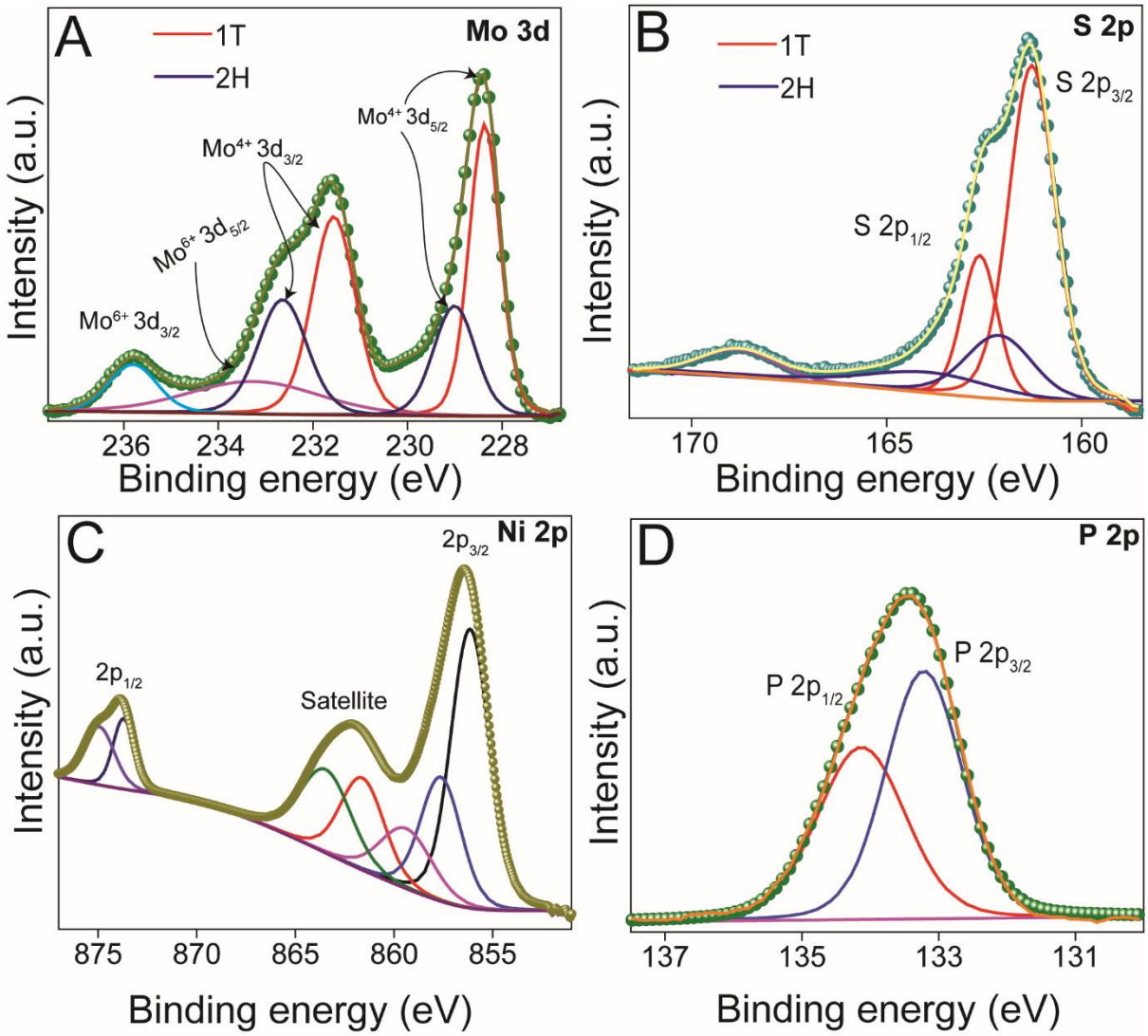

Fig. S16. High resolution X-ray photoelectron spectroscopy (XPS) plot of (**A**) Mo 3d, (**B**) S 2p, (C) Ni 2p, and (D) P 2p for 1T-$Ni_{0.2}Mo_{0.8}S_{1.8}P_{0.2}$ after long-term chronoampero metric stability test.

Table S1. Elemental composition of the catalyst obtained from AAS and ICP-OES.

Sample	Technique	Mo (at. %)	S (at. %)	Ni (at. %)	P (at. %)
1T-$Ni_{0.2}Mo_{0.8}S_{1.8}P_{0.2}$ NFs	AAS	26.9	59.7	6.8	6.6
1T-$Ni_{0.2}Mo_{0.8}S_{1.8}P_{0.2}$ NFs	ICP-OES	25.8	60.4	7.1	6.7
1T-$Ni_{0.2}Mo_{0.8}S_{1.8}P_{0.2}$ NS/CC	AAS	27.1	59.5	6.5	6.9
1T-$Ni_{0.2}Mo_{0.8}S_{1.8}P_{0.2}$ NS/CC	ICP-OES	26.4	59.9	6.9	6.8
$Ni_{0.1}Mo_{0.9}S_{1.8}P_{0.2}$	ICP-OES	30.1	60.4	3.2	6.3
$Ni_{0.3}Mo_{0.7}S_{1.8}P_{0.2}$	ICP-OES	22.6	60.7	9.7	7.0
$Ni_{0.2}Mo_{0.8}S_{1.7}P_{0.3}$	ICP-OES	26.7	56.4	6.7	10.2
$Ni_{0.2}Mo_{0.8}S_{1.9}P_{0.1}$	ICP-OES	26.4	63.6	6.6	3.4
$Ni_{0.1}Mo_{0.9}S_{1.7}P_{0.3,}$	ICP-OES	30.2	56.2	3.4	10.2
$Ni_{0.1}Mo_{0.9}S_{1.9}P_{0.1,}$	ICP-OES	30.1	63.1	3.3	3.5
$Ni_{0.3}Mo_{0.7}S_{1.7}P_{0.3,}$	ICP-OES	23.5	56.5	10.1	9.9
$Ni_{0.3}Mo_{0.7}S_{1.9}P_{0.1}$	ICP-OES	23.3	63.5	10.3	2.9

Table S2. Comparison table towards HER performances with recently reported catalysts.

Catalysts	HER overpotential (mV) @ 10 mA cm^{-2}	Reference
1T-$Ni_{0.2}Mo_{0.8}S_{1.8}P_{0.2}$ NS/CC	55	**This Work**
1T-$Ni_{0.2}Mo_{0.8}S_{1.8}P_{0.2}$ NFs	99	**This Work**
1T/2H MoS_2	220	S1
P-doped 2H-MoS_2	217	S2
MoS_2/Mo	198	S3
Defect-rich MoS_2	195	S4
MoS_2 nanodots	248	S5
Co-$^{s}MoS_2$	220	S6
Co_9S_8@MoS_2	342	S7
MoS_x flat boxes	206	S8
$CoMoS_3$ hollow prisms	171	S9
MoO_x/MoS_2	170	S10

Table S3. Comparison table towards OER performances with recently reported catalysts.

Catalysts	OER overpotential (mV)	Reference
1T-$Ni_{0.2}Mo_{0.8}S_{1.8}P_{0.2}$ NS/CC	286 (@ 40 mA cm^{-2})	**This Work**
1T-$Ni_{0.2}Mo_{0.8}S_{1.8}P_{0.2}$ NFs	305 (@ 40 mA cm^{-2})	**This Work**
MoS_2-Ni_3S_2/NF	249 (@ 10 mA cm^{-2})	S11
MoS_2/Ni_3S_2	218 (@ 10 mA cm^{-2})	S12
MoS_2/Ni	250 (@ 10 mA cm^{-2})	S13
Co/Ni-1T-MoS_2	235 (@ 10 mA cm^{-2})	S14
CoS-$Co(OH)_2$/MoS_{2+x}	380 (@ 10 mA cm^{-2})	S15
Co_3O_4@MoS_2	269 (@ 10 mA cm^{-2})	S16
Co_9S_8@MoS_2	342 (@ 10 mA cm^{-2})	S17
Ni-Fe-LDH/MoS_2	250 (@ 10 mA cm^{-2})	S18
MoS_2/QD	370 (@ 10 mA cm^{-2})	S19
$FeNiO_x(OH)_y$@MoS_2/rGO	240 (@ 10 mA cm^{-2})	S20

Table S4. Comparison table of cell voltages for overall water splitting with some recently reported catalysts.

Catalysts	Cell voltages for overall water splitting (V)	Reference
1T-$Ni_{0.2}Mo_{0.8}S_{1.8}P_{0.2}$ NS/CC (+ –)	1.52 (@ 10 mA cm^{-2})	**This work**
1T-$Ni_{0.2}Mo_{0.8}S_{1.8}P_{0.2}$ NFs (+ –)	1.53 (@ 10 mA cm^{-2})	**This work**
NiSe (+ –)	1.63 (@ 10 mA cm^{-2})	S21
Ni_5P_4 (+ –)	1.7 (@ 10 mA cm^{-2})	S22
Co-P (+ –)	1.65 (@ 10 mA cm^{-2})	S23
Ni_2P NPs (+ –)	1.63 (@ 10 mA cm^{-2})	S24
NiFe LDH (+ –)	1.7 (@ 10 mA cm^{-2})	S25
$Ni_{0.9}Fe_{0.1}$/NC (+ –)	1.64 (@ 10 mA cm^{-2})	S26
MoS_2/Ni_3S_2 (+ –)	1.56 (@ 10 mA cm^{-2})	S27
$Co_{0.7}Fe_{0.3}P$/CNTs (+ –)	1.49 (@ 10 mA cm^{-2})	S28
Co-MoS_2/BCCF-21 (+ –)	1.55 (@ 10 mA cm^{-2})	S29
Ni@NC-800 (+ –)	1.62 (@ 10 mA cm^{-2})	S30
CoP/NCNHP (+ –)	1.64 (@ 10 mA cm^{-2})	S31
CoS-$Co(OH)_2/MoS_{2+x}$ (+ –)	1.58 (@ 10 mA cm^{-2})	S32
Co_3O_4@MoS_2 (+ –)	1.59 (@ 10 mA cm^{-2})	S33
CoMoNiS-NF-31 (+ –)	1.54 (@ 10 mA cm^{-2})	S34
MoS_2/NiCoS (+ –)	1.50 (@ 10 mA cm^{-2})	S35
Co/Ni-T-MoS_2 (+ –)	1.44 (@ 10 mA cm^{-2})	S14

References

1 Z. Liu, Z. Gao, Y. Liu, M. Xia, R. Wang and N. Li, *ACS Appl. Mater. Interfaces*, 2017, **9**, 25291–25297.

2 X. Huang, M. Leng, W. Xiao, M. Li, J. Ding, T. L. Tan, W. S. V. Lee and J. Xue, *Adv. Funct. Mater.*, 2017, **27**, 1604943.

3 J. Li, J. Kang, Q. Cai, W. Hong, C. Jian, W. Liu and K. Banerjee, *Adv. Mater. Interfaces*, 2017, **4**, 1–7.

4 J. Benson, M. Li, S. Wang, P. Wang and P. Papakonstantinou, *ACS Appl. Mater.*

Interfaces, 2015, **7**, 14113–14122.

5 D. Gopalakrishnan, D. Damien and M. M. Shaijumon, *ACS Nano*, 2014, **8**, 5297–5303.

6 Y. Li, J. Wang, X. Tian, L. Ma, C. Dai, C. Yang and Z. Zhou, *Nanoscale*, 2016, **8**, 1676–1683.

7 J. Bai, T. Meng, D. Guo, S. Wang, B. Mao and M. Cao, *ACS Appl. Mater. Interfaces*, 2018, **10**, 1678–1689.

8 L. Yu, B. Y. Xia, X. Wang and X. W. Lou, *Adv. Mater.*, 2016, **28**, 92–97.

9 C. Wu, B. Liu, J. Wang, Y. Su, H. Yan, C. Ng, C. Li and J. Wei, *Appl. Surf. Sci.*, 2018, **441**, 1024–1033.

10 G. Zhang, Y. S. Feng, W. T. Lu, D. He, C. Y. Wang, Y. K. Li, X. Y. Wang and F. F. Cao, *ACS Catal.*, 2018, **8**, 5431–5441.

11 Y. Yang, K. Zhang, H. Lin, H.C. Chan, L. Yang, and Q. Gao, *ACS Catal.*, 2017, **7**, 2357-2366.

12 J. Zhang, T. Wang, D. Pohl, B. Rellinghaus, R. Dong, S. Liu, X. Zhuang and X. Feng, 2016, **55**, 6702–6707.

13 K. Yan and Y. Lu, *Small*, 2016, **12**, 2975–2981.

14 H. Li, S. Chen, X. Jia, B. Xu, H. Lin, H. Yang, L. Song and X. Wang, *Nat. Commun.*, 2017, **8**, 1–11.

15 T. Yoon and K. S. Kim, *Adv. Funct. Mater.*, 2016, **26**, 7386–7393.

16 J. Liu, J. Wang, B. Zhang, Y. Ruan, H. Wan, X. Ji, K. Xu, D. Zha, L. Miao and J. Jiang, *J. Mater. Chem. A*, 2018, **6**, 2067–2072.

17 M. S. Islam, M. Kim, X. Jin, S. M. Oh, N. S. Lee, H. Kim and S. J. Hwang, *ACS Energy Lett.*, 2018, **3**, 952–960.

18 B. Mohanty, M. Ghorbani-Asl, S. Kretschmer, A. Ghosh, P. Guha, S. K. Panda, B. Jena, A. V. Krasheninnikov and B. K. Jena, *ACS Catal.*, 2018, **8**, 1683–1689.

19 C. G. Morales-Guio, L. Liardet, M. T. Mayer, S. D. Tilley, M. Grätzel and X. Hu, *Angew. Chemie - Int. Ed.*, 2015, **54**, 664–667.

20 F. Zhou, X. Zhang, R. Sa, S. Zhang, Z. Wen and R. Wang, *Chem. Eng. J.*, 2020, **397**, 125454.

21 C. Tang, N. Cheng, Z. Pu, W. Xing and X. Sun, *Angew. Chemie - Int. Ed.*, 2015, **54**, 9351–9355.

22 M. Ledendecker, S. Krickcalderõn, C. Papp, H. P. Steinrück, M. Antonietti and M. Shalom, *Angew. Chemie - Int. Ed.*, 2015, **54**, 12361–12365.

23 N. Jiang, B. You, M. Sheng and Y. Sun, *Angew. Chemie - Int. Ed.*, 2015, **54**, 6251–6254.

24 L. A. Stern, L. Feng, F. Song and X. Hu, *Energy Environ. Sci.*, 2015, **8**, 2347–2351.

25 J. Luo, J. H. Im, M. T. Mayer, M. Schreier, M. K. Nazeeruddin, N. G. Park, S. D. Tilley, H. J. Fan and M. Grätzel, *Science*, 2014, **345**, 1593–1596.

26 X. Zhang, H. Xu, X. Li, Y. Li, T. Yang and Y. Liang, *ACS Catal.*, 2016, **6**, 580–588.

27 Y. Yang, K. Zhang, H. Lin, X. Li, H. C. Chan, L. Yang and Q. Gao, *ACS Catal.*, 2017, **7**, 2357–2366.

28 X. Zhang, X. Zhang, H. Xu, Z. Wu, H. Wang and Y. Liang, *Adv. Funct. Mater.*, 2017, **27**, 1–12.

29 Q. Xiong, Y. Wang, P. F. Liu, L. R. Zheng, G. Wang, H. G. Yang, P. K. Wong, H. Zhang and H. Zhao, *Adv. Mater.*, 2018, **30**, 1–7.

30 X. Ge, L. Chen, L. Zhang, Y. Wen, A. Hirata and M. Chen, *Adv. Mater.*, 2014, **26**, 3100–3104.

31 Y. Pan, K. Sun, S. Liu, X. Cao, K. Wu, W. C. Cheong, Z. Chen, Y. Wang, Y. Li, Y. Liu, D. Wang, Q. Peng, C. Chen and Y. Li, *J. Am. Chem. Soc.*, 2018, **140**, 2610–2618.

32 H. Lin, H. Li, Y. Li, J. Liu, X. Wang and L. Wang, *J. Mater. Chem. A*, 2017, **5**, 25410–25419.

33 Y. Luo, X. Li, X. Cai, X. Zou, F. Kang, H. M. Cheng and B. Liu, *ACS Nano*, 2018, **12**, 4565–4573.

34 Y. Yang, H. Yao, Z. Yu, S. M. Islam, H. He, M. Yuan, Y. Yue, K. Xu, W. Hao, G. Sun, H. Li, S. Ma, P. Zapol and M. G. Kanatzidis, *J. Am. Chem. Soc.*, 2019, **141**, 10417–10430.

35 C. Qin, A. Fan, X. Zhang, S. Wang, X. Yuan and X. Dai, *J. Mater. Chem. A*, 2019, **7**, 27594–27602.